AIAA AVIATION Forum
17-21 June 2019, Dallas, Texas
AIAA Aviation 2019 Forum

10.2514/6.2019-3652

Study of Super-Lift Coefficient of Co-Flow Jet Airfoil and Its Power Consumption

Yang Wang *Yunchao Yang † Gecheng Zha ‡
Dept. of Mechanical and Aerospace Engineering
University of Miami, Coral Gables, Florida 33124
E-mail: gzha@miami.edu

Abstract

This paper studies the super-lift coefficient of Co-Flow Jet (CFJ) airfoil and its power consumption. An optimized CFJ airfoil (CFJ6421-SST150-SUC247-INJ117) for cruise with enlarged injection slot size can achieve higher maximum lift coefficient than the baseline CFJ airfoil (CFJ6421-SST016-SUC053-INJ009), but at substantially lower power consumption. The reason is that the CFJ power consumption is determined linearly by the mass flow rate, but exponentially by the total pressure ratio. The larger injection slot size yields greater C_μ, higher mass flow rate, and lower injection jet velocity, which generate much smaller flow energy loss, lower total pressure ratio, and hence substantially reduces the CFJ power consumption. For example, at a C_{Lmax} of 9, the total pressure ratio is reduced from 4.2 to 1.3 while the injection slot size is increased from 0.09%C to 1.17%C. The power coefficient is reduced by 5 times. Such phenomenon applies to all active flow control using fluidic actuators. The flow vortex structures are studied by comparing the flow from AoA of 30° to 80°. The flows are all attached. At an AoA below 60°, the vortex structures on the CFJ airfoil suction surface are primarily three layers, 1) a clockwise layer due to the wall boundary layer; 2) a counter-clockwise layer due to the high speed jet; and 3) the second clockwise vortex layer shed from the leading wall boundary layer, which is dissipated quickly downstream of the injection slot. However, when the flow reaches the stall AoA of 65° with the maximum lift coefficient and adverse pressure gradient, the second clockwise vortex layer is erupted with a substantially enlarged area, which contributes significantly to the ultra-high lift generation. The vortex structures become four counter-rotating vortex layers as previously observed by Yang and Zha. The overall conclusion is that a CFJ airfoil with a large injection slot size is preferred. It is as effective to enhance lift, generate thrust, and increase stall AoA, but at a substantially lower power consumption. It makes the same CFJ airfoil with fixed geometry applicable to the whole flight envelop from takeoff/landing to cruise.

Nomenclature

CFJ	Co-flow jet
AoA	Angle of attack
LE	Leading Edge
TE	Trailing Edge
S	Planform area
c	Airfoil chord
U	Flow velocity

* Graduate Student, AIAA student member
† Ph.D candidate, current postdoc at University of Florida
‡ Professor, ASME Fellow, AIAA associate Fellow

q	Dynamic pressure $0.5\,\rho\,U^2$
p	Static pressure
ρ	Air density
$\dot{m}$	Mass flow
M	Mach number
ω	Pitching Moment
P	Pumping power
∞	Free stream conditions
$_j$	Jet conditions
C_L	Lift coefficient $L/(q_\infty\,S)$
C_{Lmax}	Maximum Lift coefficient at a constant C_μ
C_D	Drag coefficient $D/(q_\infty\,S)$
C_μ	Jet momentum coef. $\dot{m}_j\,U_j/(q_\infty\,S)$
$(C_L/C_D)_c$	CFJ airfoil corrected aerodynamic efficiency $L/(D+\,P/V_\infty)$
Pc	Power coefficient $L/(q_\infty\,S\,V_\infty)$
M_{is}	Isentropic Mach Number
M_∞	Freestream Mach Number
P_{tinj}	Total injection pressure
P_{tsuc}	Total suction pressure
PR	Pressure ratio of P_{tinj} and P_{tsuc}

1 Introduction

The maximum lift coefficient, C_{Lmax}, is an important factor to determine aircraft takeoff and landing performance. A high C_{Lmax} will yield low stall velocity, shorter run way, and low airframe noise. To overcome the complexity and high cost of conventional high lift flap systems, active flow control provides attractive new options.

Lefebvre and Zha [1] designed a CFJ airfoil, CFJ6421-SST150-SUC133-INJ065, which is modified from the NACA 6421 airfoil. In the CFJ airfoil name convention, the SST150 means the airfoil has its suction surface translation (SST) downward by 1.5%C from the baseline NACA 6421 airfoil. The INJ065 stands for that the airfoil has an injection slot size of 0.65%C. The SUC133 stands for that the airfoil has the suction slot size of 1.33%C. A wing with aspect ratio of 20 using that airfoil achieves an excellent cruise performance with a cruise lift coefficient of 1.22 and a corrected aerodynamic efficiency of 25.2 at AoA of 5° and C_μ of 0.04. The 3D wing obtains a C_{Lmax} at takeoff and landing of 4.7 at AoA of 40° and C_L of 0.28. This is a very well performed airfoil for both cruise and takeoff/landing.

The 21% thickness CFJ airfoil is further redesigned by Yang and Zha [2] with a substantially reduced injection and suction sizes, namely CFJ6421-SST016-SUC053-INJ009, which achieves a maximum C_L of 12.6 at AoA of 70° and C_μ of 0.60 with a significantly increased power consumption as shown in Fig. 1, which shows a logarithm relationship between the maximum lift coefficient C_{Lmax} and power coefficient Pc for different CFJ airfoils. The C_{Lmax} increases linearly with the increases of the Pc at the beginning, as the Pc keeps increasing, the C_{Lmax} appears to reach its plateau of 14. The theoretical C_{Lmax} based on the potential flow theory of Smith [3] is determined by:

$$C_{Lmax} = 2\pi(1 + t/c) \tag{1}$$

where the t/c is the ratio of the maximum airfoil thickness to the chord. This C_{Lmax} limit of the potential flow is obtained at AoA of 90° since a potential flow will have no flow separation and stall [3]. For the 21% thickness airfoil, the maximum lift coefficient limit is 7.6 based on Eq. (1). Fig. 1 clearly indicates that the CFJ airfoil can exceed this limit by far. The lift coefficient is hence named super-lift coefficient [2]. As aforementioned, the injection size is reduced to 0.09%C to achieve a super-lift coefficient with high injection momentum at a price of substantially increased power coefficient.

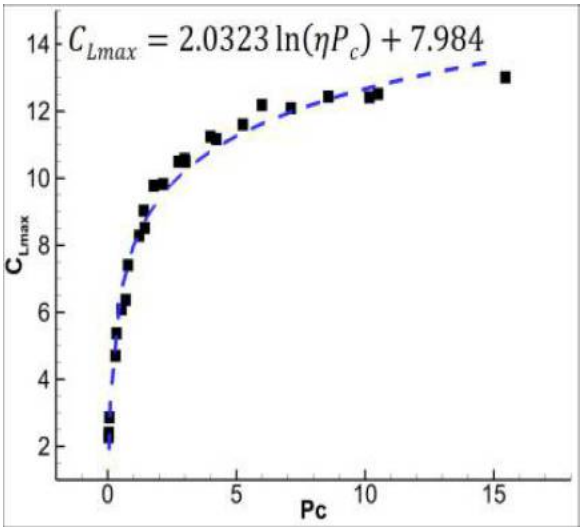

Figure 1: Variation of C_{Lmax} with Pc for different CFJ airfoils.

It is desirable to have a Co-Flow Jet airfoil for the whole flight envelop without varying the slot size for high C_{Lmax} at takeoff/landing and high aerodynamic efficiency at cruise. Overall, a large slot size is very beneficial to have high cruise efficiency due to reduced CFJ power coefficient. The question we want to ask then becomes: Can a super-lift coefficient still be achieved using a large injection slot size fixed at the cruise condition with a reduced power coefficient? The motivation of this paper is to answer this question.

The Super-Lift Coefficient capability of CFJ airfoil is proved experimentally in wind tunnel testing in 2018 by Zha et al.[4]. However, in both of the SLC studies[2, 4], the CFJ power consumption at SLC is not the focus since the priority is to investigate and prove the aerodynamic performance. Power consumption and energy expenditure of a lift enhancement technology is crucial, because ultimately they determine the aircraft system efficiency, the amount of energy source to be carried, and the gross weight of the aircraft.

The power consumption is determined by the jet mass flow and total enthalpy change as the following:

$$P = \dot{m}(H_{t1} - H_{t2}) \tag{2}$$

where H_{t1} and H_{t2} are the mass-averaged total enthalpy in the injection cavity and suction cavity respectively, P is the Power required by the pump and $\dot{m}$ the jet mass flow rate. Using the mass-averaged total pressure P_{t1} and P_{t2} in the injection and suction cavity respectively, the pump efficiency η, and the total pressure ratio of the pump $\Gamma = \frac{P_{t1}}{P_{t2}}$, the CFJ power consumption is expressed as:

$$P = \frac{\dot{m} C_p T_{t2}}{\eta} (\Gamma^{\frac{\gamma-1}{\gamma}} - 1) \tag{3}$$

where γ is the specific heat ratio equal to 1.4 for air. The power coefficient is expressed as:

$$P_c = \frac{P}{\frac{1}{2}\rho_\infty V_\infty^3 S} \tag{4}$$

As indicated in Eq. (3), the CFJ power consumption is determined linearly by the mass flow rate ($\dot{m}$) and exponentially by the total pressure ratio (Γ). This is actually true for general flow control methods relying on fluidic actuators such as circulation control (CC) airfoil. However, since CC airfoil is not mass conservative within the controlled airfoil system, it needs to introduce air flow from other sources, typically from the engine bleed. In that case, the amount of mass flow must be minimized since a high engine bleed mass hurts the engine performance significantly. Further more, introducing air flow from the engine typically needs to take a winding long way, which could incur high energy loss and hence require high total pressure ratio. In general, the CC airfoil flow control usually experiences high energy expenditure.

For CFJ airfoil, the amount of mass flow is not an issue since it is a zero-net-mass-flux flow control. To reduce the power consumption, it is more effective to increase the jet mass flow and reduce the total pressure ratio for its exponential effect. The objective of this paper is to demonstrate that the CFJ airfoil with enlarged injection slot size optimized for cruise condition can achieve super-lift coefficient with substantially reduced total pressure ratio and thus the reduced power consumption.

2 Definitions

This section defines the parameters to be used to describe the performance of CFJ airfoil.

2.1 Lift and Drag Calculation

The momentum and pressure at the injection and suction slots produce a reactionary force, which is automatically measured by the force balance in wind tunnel testing. However, for CFD simulation, the full reactionary force needs to be included. Using control volume analysis, the reactionary force can be calculated using the flow parameters at the injection and suction slot opening surfaces. Zha et al. [5] give the following formulations to calculate the lift and drag due to the jet reactionary force for a CFJ airfoil. By considering the effects of injection and suction jets on the CFJ airfoil, the expressions for these reactionary forces are given as :

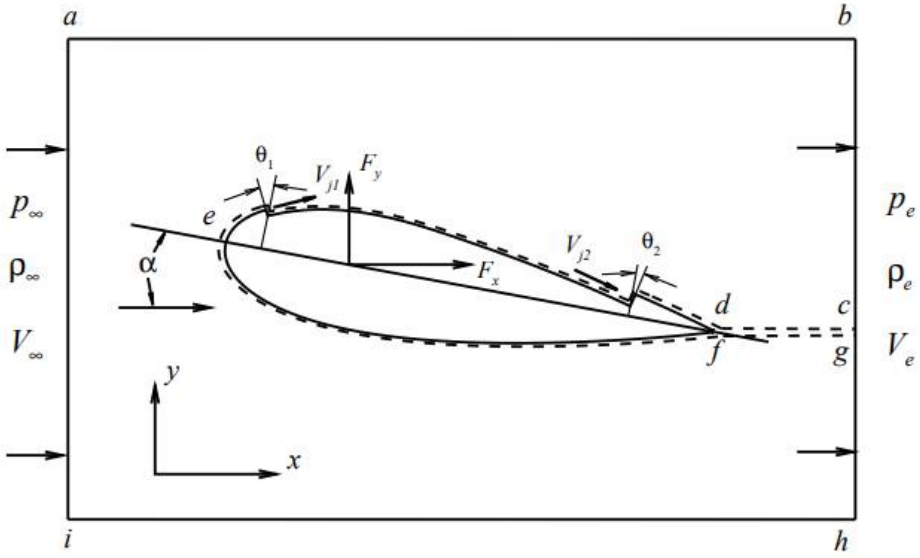

Figure 2: The control volume for a CFJ airfoil.

$$F_{x_{cfj}} = (\dot{m}_j V_{j1} + p_{j1} A_{j1}) * cos(\theta_1 - \alpha) - (\dot{m}_j V_{j2} + p_{j2} A_{j2}) * cos(\theta_2 + \alpha) \tag{5}$$

$$F_{y_{cfj}} = (\dot{m}_{j1} V_{j1} + p_{j1} A_{j1}) * sin(\theta_1 - \alpha) + (\dot{m}_{j2} V_{j2} + p_{j2} A_{j2}) * sin(\theta_2 + \alpha) \tag{6}$$

where the subscripts 1 and 2 stand for the injection and suction respectively, and θ_1 and θ_2 are the angles between the injection and suction slot's surface and a line normal to the airfoil chord. α is the angle of attack.

The total lift and drag on the airfoil can then be expressed as:

$$D = R'_x - F_{x_{cfj}} \tag{7}$$

$$L = R'_y - F_{y_{cfj}} \tag{8}$$

where R'_x and R'_y are the surface integral of pressure and shear stress in x (drag) and y (lift) direction excluding the internal ducts of injection and suction. For CFJ wing simulations, the total lift and drag are calculated by integrating Eqs. (7) and (8) in the spanwise direction.

2.2 Jet Momentum Coefficient

The jet momentum coefficient C_μ is a parameter used to quantify the jet intensity. It is defined as:

$$C_\mu = \frac{\dot{m} V_j}{\frac{1}{2} \rho_\infty {V_\infty}^2 S} \tag{9}$$

where $\dot{m}$ is the injection mass flow, V_j is the mass-averaged injection velocity, ρ_∞ and V_∞ denote the free stream density and velocity, and S is the planform area.

2.3 Corrected Aerodynamic Efficiency

The conventional wing aerodynamic efficiency is defined as:

$$\frac{L}{D} \tag{10}$$

For the CFJ wing, the ratio above still represents the pure aerodynamic relationship between lift and drag. However since CFJ active flow control consumes energy, the ratio above is modified to take into account the energy consumption of the pump. The formulation of the corrected aerodynamic efficiency for CFJ wings is:

$$(\frac{L}{D})_c = \frac{C_L}{C_D + P_c} \tag{11}$$

where V_∞ is the free stream velocity, P is the pumping power, and L and D are the lift and drag generated by the CFJ wing. The formulation above converts the power consumed by the CFJ into a force $\frac{P}{V_\infty}$ which is added to the aerodynamic drag D. If the pumping power is set to 0, this formulation returns to the aerodynamic efficiency of a conventional wing.

2.4 Aircraft Productivity

To compare aircraft that have the same ratio of initial weight to final weight with the same engine fuel consumption or battery energy density, the productivity efficiency C_L^2/C_D is introduced to measure the productivity of an airplane represented by its range multiplied by its weight [2].

The productivity efficiency $C_L^2/C_D = C_L(C_L/C_D)$ is a more comprehensive parameter than the conventional aerodynamic efficiency C_L/C_D to measure the merit of an airplane aerodynamic design for cruise performance. The former includes not only the information of C_L/C_D, but also the information of the aircraft weight C_L. For example, for two airplane designs having the same C_L/C_D with one C_L twice larger than the other, if the wing sizes are the same, one airplane will be able to carry twice more weight than the other with productivity and wing loading increased by 100%. Such a large difference is not reflected by C_L/C_D, but very well reflected by C_L^2/C_D.

The definition of C_L/C_D in general is a suitable measure of merit for conventional aircraft design. This is because at a certain Mach number regime, the maximum C_L/C_D is usually achieved at low angle of attack within the drag bucket and is more or less the same for different airfoil designs. In other words, for the same optimum C_L/C_D, the C_L is about the same. A typical C_L for subsonic airfoil is about 0.4 and for transonic airfoil is about 0.7.

For CFJ airfoil, the minimum CFJ pumping power occurs at a fairly high AoA [6, 7]. With the augmentation of CFJ, the subsonic cruise lift coefficient of a CFJ airfoil is typically 2 to 3 times higher than the conventional airfoil with about the same $(C_L/C_D)_c$ [1]. Such a high lift coefficient is unattainable for conventional airfoil since they would be either stalled or near stalled with very high drag. Hence for CFJ aircraft design, the productivity efficiency $C_L^2/C_D = C_L(C_L/C_D)$ is more informative to be used to reflect the aerodynamic performance. The corrected productivity efficiency for CFJ airfoils is $(C_L^2/C_D)_c = C_L^2/(C_D + P_c)$.

3 CFD Simulation Setup

The in house FASIP (Flow-Acoustics-Structure Interaction Package) CFD code is used to conduct the numerical simulation. The 3D Reynolds Averaged Navier-Stokes (RANS) equations with one-equation Spalart-Allmaras [8] turbulence model is used. A 3rd order WENO scheme for the inviscid flux [9, 10, 11, 12, 13, 14] and a 2nd order central differencing for the viscous terms [9, 13] are employed to discretize the Navier-Stokes equations. The low diffusion E-CUSP scheme used as the approximate Riemann solver suggested by Zha et al [10] is utilized with the WENO scheme to evaluate the inviscid fluxes. Implicit time marching method using Gauss-Seidel line relaxation is used to achieve a fast convergence rate [15]. Parallel computing is implemented to save wall clock simulation time [16].

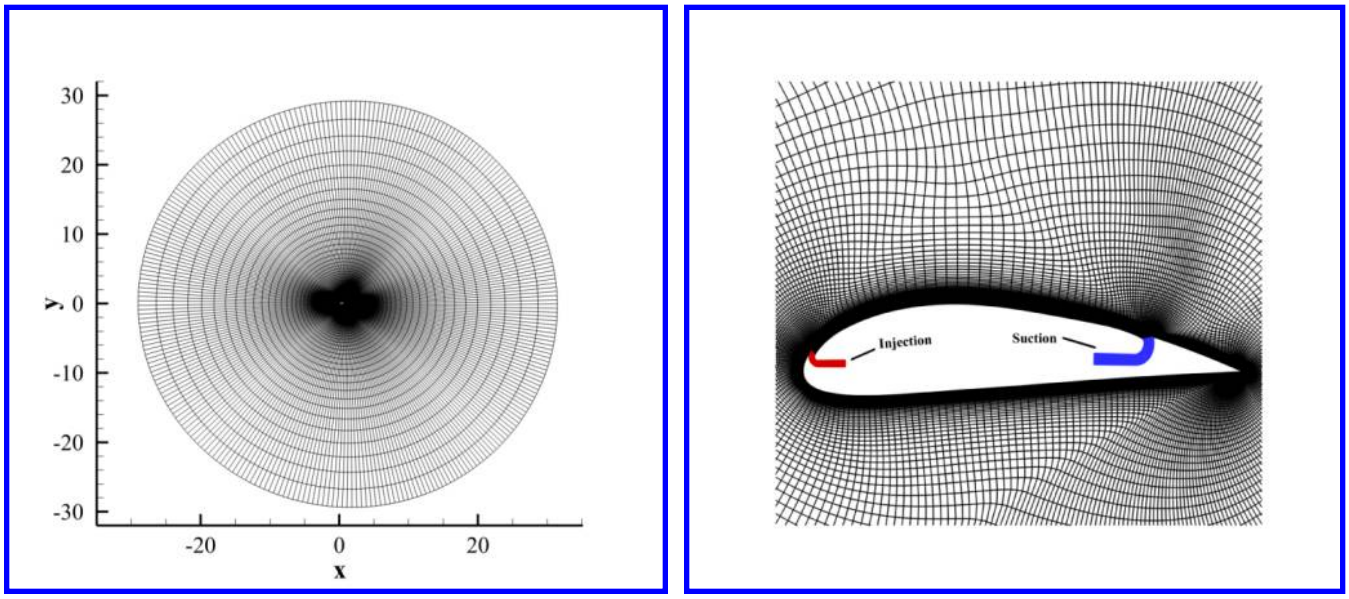

Figure 3: Computational mesh used in the current work.

3.1 Boundary Conditions

The 3rd order accuracy no slip condition is enforced on the solid surface with the wall treatment suggested by Shen et al. [17] to achieve the flux conservation on the wall. The computational mesh is shown in Fig. 3. The ducts geometries are predetermined according to our previous designs. Total pressure, total temperature and flow angles are specified at the injection duct inlet, as well as the upstream portion of the far field. Constant static pressure is applied at the suction duct outlet as well as the downstream portion of the far field. The total mesh size is 47,200 points, split into 10 domains for parallel computation. The first grid point on the wing surface is placed at $y^+ \approx 1$. This mesh size is the same as the mesh size used by Yang and Zha in [2].

4 Results and Discussion

The high lift CFJ airfoil designed by Yang and Zha [2] is used as the baseline for reference for reducing the power consumption while keeping the same high lift coefficient. As aforementioned, a fluid actuator power is linearly determined by the mass flow rate and exponentially determined by the total pressure ratio. Thus the

most effective way to reduce the CFJ power consumption is to reduce the flow energy loss, specifically the total pressure ratio that is required to sustain the CFJ. In fluid mechanics, if a certain amount of mass flow is to be dumped to a large space via a hole, a smaller size hole will cause more energy loss than a large size hole [18]. It is hence expected that a large injection size CFJ airfoil may have lower power consumption than a smaller size CFJ airfoil. However, the limit is that the injection slot size should not be too large that it does not generate sufficient velocity and momentum to enhance lift. The second limit is that both the injection and suction slot should not be choked since the flow loss will be increased significantly when it reaches sonic speed at the slot and becomes supersonic downstream. The third limit is from the airfoil geometry itself that there should be enough room to fit the injection and suction slot. The suction slot is typically 1.5 to 2 times larger than the injection slot to ensure that it will withdraw all the mass flow ejected upstream.

5 The CFJ Airfoil for Cruise with Fixed Geometry

The CFJ6421-SST150-SUC247-INJ117 airfoil optimized for cruise performance by Wang and Zha [19, 20] is studied in this paper to investigate its performance and power consumption at super-lift coefficient conditions. The purpose is to answer the question weather a fixed geometry airfoil can be used for both cruise and takeoff/landing. This airfoil is the focus of this study and is termed CFJ 2. For simplicity, the baseline airfoil from Yang and Zha [2] is termed CFJ 3. The CFJ 1 refers to the airfoil developed by Lefebvre and Zha [1], which is used as another baseline airfoil with the injection and suction slots larger than those of the baseline airfoil (CFJ 3), but smaller than those of the CFJ 2 airfoil. Table. 1 lists the three airfoil geometry parameters, which indicates that the CFJ 2 airfoil has a suction surface translation (SST) of 1.50%C, 2.7 times larger than that of the CFJ 3 airfoil, the injection slot size is 1.17%C, 80% larger than that of CFJ 1 airfoil and 13 times larger than that of the CFJ 3 airfoil, and the suction slot size is 2.47%C, 86% larger than that of CFJ 1 airfoil and 4.7 times larger than that of CFJ 3 airfoil. The questions we want to ask are: 1) Can the CFJ airfoil with such a larger slot size still achieve ultra-high lift coefficient? 2) How is the power consumption?

Table 1: Airfoil geometry parameters.

Airfoil	SST (%C)	INJ (%C)	SUC (%C)
CFJ6421-SST150-SUC133-INJ065 (CFJ 1) [1]	1.50	0.65	1.33
CFJ6421-SST150-SUC247-INJ117 (CFJ 2) [19, 20]	1.50	1.17	2.47
CFJ6421-SST016-SUC053-INJ009 (CFJ 3) [2]	0.56	0.09	0.53

6 Simulated Cases

Table. 2 lists the freestream conditions simulated in this study. They are at a constant freestream Mach number of 0.063, AoA is ranged from 10° to 80° to achieve SLC, and the C_μ is ranged from 0.04 to 3.3. The C_{Lmax} is recorded as the maximum lift coefficient of the CFJ airfoil at its stall AoA at a given C_μ value.

Table 2: Simulation cases used in the current work

Cases	Mach	AoA	C_μ
CFJ6421-SST150-SUC133-INJ065 (CFJ 1)	0.063	10°-80°	0.04 - 3.3
CFJ6421-SST150-SUC247-INJ117 (CFJ 2)	0.063	10°-80°	0.04 - 3.3
CFJ6421-SST016-SUC053-INJ009 (CFJ 3)	0.063	10°-80°	0.04 - 3.3

7 Performance of CFJ Airfoils

Fig. 4 (a) shows that the C_{Lmax} is increased with C_μ for all the three CFJ airfoils. Both CFJ 1 and CFJ 2 airfoil with the large injection slot size have no difficulties in achieving SLC. The C_{Lmax} is actually higher than that of CFJ 3 airfoil because that the injection slot can pass more flow before it is choked, but the slope of the large injection slot CFJ airfoil is smaller with the one for CFJ 2 airfoil the smallest. It means that to achieve the same C_{Lmax}, the CFJ 2 airfoil needs a higher C_μ. Fig. 4 (b) and (c) show that the drag and the nose-down pitching moment coefficient of the CFJ 2 airfoil are substantially smaller than those of the CFJ 3 airfoil. This is the benefit of the larger injection slot size. Overall, the CFJ 1 and 2 airfoil with large injection slot size behave similarly.

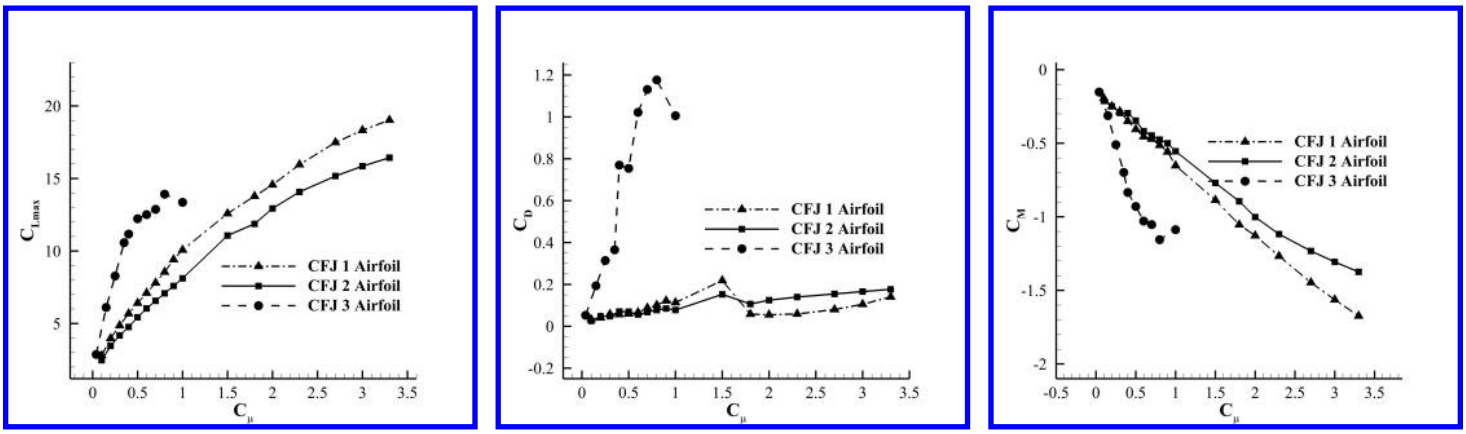

(a) (b) (c)

Figure 4: Lift, drag and moment coefficients for CFJ airfoil 1, 2, and 3.

The C_{Lmax}/C_D, $(C_{Lmax}/C_D)_c$ and $({C_{Lmax}}^2/C_D)_c$ plots at $C_L = C_{Lmax}$ for all the three CFJ airfoils are plotted in Fig. 5. The CFJ 2 airfoil has the highest corrected aerodynamic efficiency of $(C_L/C_D)_C$. The advantage at low C_μ is particularly large. All these are attributed to the very low total pressure ratio (PR) with the maximum value no greater than 1.3 as shown in Fig. 6 (c), substantially lower than that of the CFJ 3 airfoil with the high total pressure ratio up to 4.2. Since CFJ provides higher C_L, the CFJ airfoil productivity efficiency ($({C_L}^2/C_D)_c$) is hence higher as shown in Fig. 5 (c). Fig. 5 (a) shows some wiggling results for CFJ 1 and CFJ 2 airfoil, it is because the C_{Lmax} occurs at different AoA, when the C_μ varies. For the CFJ 2 airfoil, the C_{Lmax} occurs at AoA of 65° when the C_μ reaches 1.8 or higher.

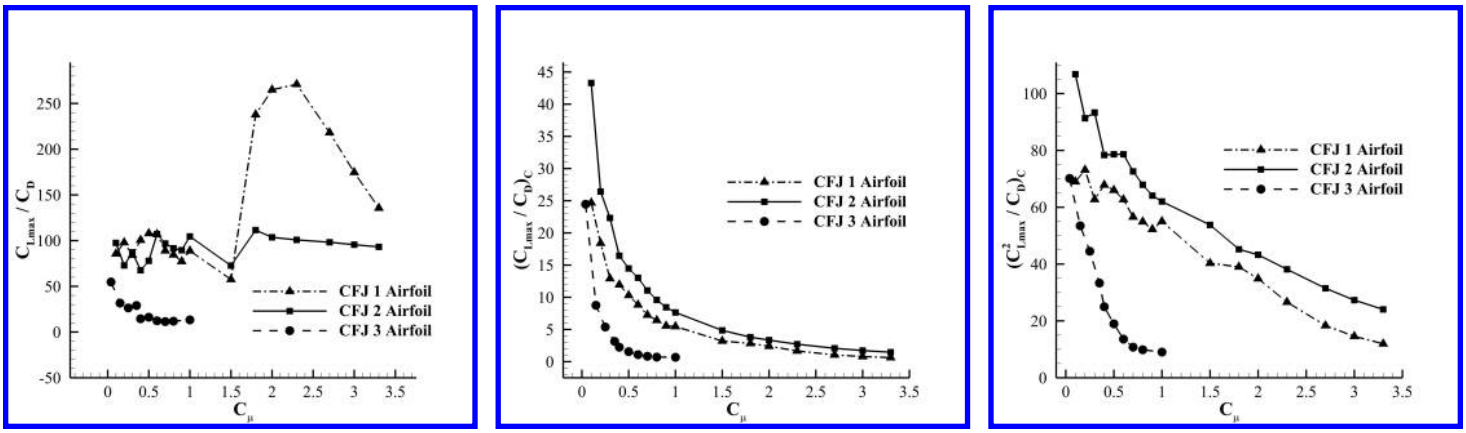

(a) (b) (c)

Figure 5: C_{Lmax}/C_D, $(C_{Lmax}/C_D)_c$, $(C_{Lmax}{}^2/C_D)_c$ plots for CFJ airfoil 1, 2, and 3.

The P_{tinj} , P_{tsuc} , and total pressure ratio PR plots for all the three CFJ airfoils are shown in Fig. 6. Fig. 6 (a) shows that the CFJ 3 airfoil with very small injection slot size requires a substantially higher injection total pressure to push the flow through. At the same time, the suction total pressure of CFJ 3 is also significantly lower than that of the CFJ 1 and CFJ 2 due to higher total pressure loss going through the very small injection slot. Benefited from the larger injection and suction slot size, the CFJ 2 airfoil has a very low total pressure ratio as shown in Fig. 6 (c), which yields the most important results of our interest: the power coefficient (P_c) variation with C_μ and C_{Lmax} as shown in Fig. 7. The power coefficient of the CFJ 2 airfoil is substantially lower than that of CFJ 3 airfoil even though the C_μ of CFJ 2 airfoil is significantly higher. For example, if both airfoils need to achieve C_{Lmax} of 10, the CFJ 3 airfoil consumes the power about 5 times more even though the C_μ is less than 1/4 of that of the CFJ 2 airfoil.

An important conclusion that is a little different from the conventional wisdom is that to achieve the same lift coefficient, a higher CFJ C_μ is preferred because it reduces the power consumption and improves the overall system efficiency. The power consumption of CFJ airfoil can be drastically reduced by enlarging the slot size, increasing the jet mass flow rate, and reducing the total pressure ratio between the injection and suction slot.

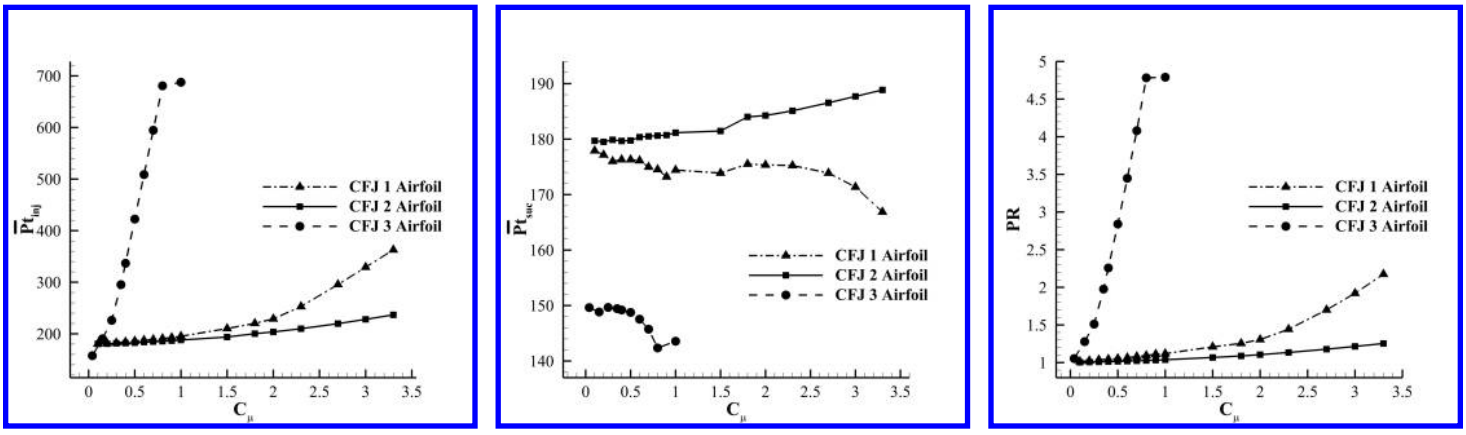

(a) (b) (c)

Figure 6: P_{tinj} , P_{tsuc} , PR plots for CFJ airfoil 1, 2, and 3.

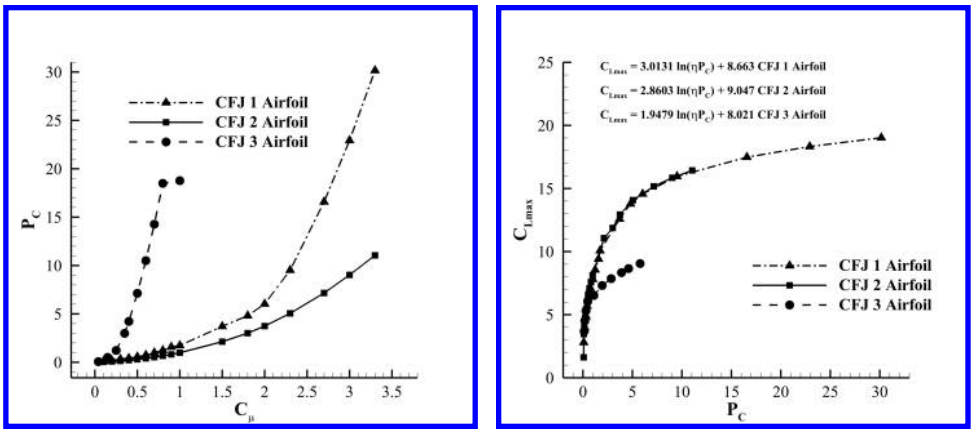

(a) (b)

Figure 7: Power coefficient (Pc), $C_{L_{max}}$ logarithm equation plots for CFJ airfoil 1, 2, and 3.

Eq. (12), Eq. (13), and Eq. (14) are the logarithm equation for CFJ 1 airfoil, CFJ 2 airfoil, and CFJ 3 airfoil respectively.

$$C_{L_{max}} = 3.0131 \ln(\eta Pc) + 8.663 \tag{12}$$

$$C_{L_{max}} = 2.8603 \ln(\eta Pc) + 9.047 \tag{13}$$

$$C_{L_{max}} = 1.9479 \ln(\eta Pc) + 8.021 \tag{14}$$

As shown in Fig. 7, CFJ 1 and CFJ 2 have similar power consumption, but CFJ 2 has substantially lower value at high C_μ. Both CFJ 1 and CFJ 2 with larger injection slots significantly outperform CFJ 3, which has a very small injection slot size. The correlation between C_L and Pc for CFJ 1 and CFJ 2 are similar as defined by Eq. (12) and Eq. (13), but they are much more efficient than the one for CFJ 3 defined by Eq. (14).

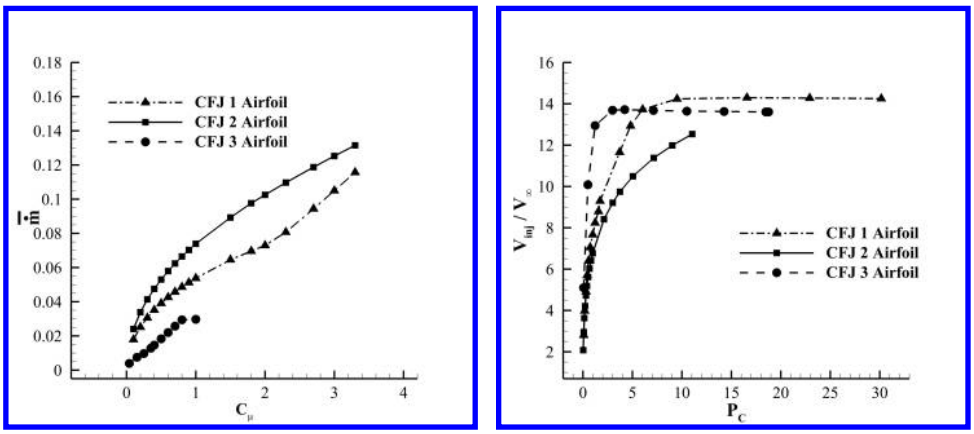

(a) (b)

Figure 8: Injection Mass flow ($\dot{m}$) and Normalized jet velocity at injection (V_{inj}) for CFJ airfoil 1, 2, and 3.

Fig. 8 shows the normalized jet mass flow rate and the ratio of injection speed to freestream speed. As shown in Fig. 8, for the same C_μ, the CFJ 2 airfoil always has substantially higher jet mass flow rate and lower injection velocity, which are the factors to substantially reduce the CFJ power.

Fig. 9 shows the Mach number contours zoomed in the injection region for CFJ 1, CFJ 2, and CFJ 3 airfoils at same lift coefficient of 12.2. The CFJ 3 has the highest the Mach number of 1.019 at the injection outlet due to the smallest injection slot size. The enlarged injection slot size of CFJ 2 airfoil has the smallest injection Mach number of 0.659. The CFJ 1 airfoil has the injection Mach number of 0.803. It is expected that the CFJ 2 airfoil will have substantially lower noise than the CFJ 3 airfoil due to the largely reduced jet velocity.

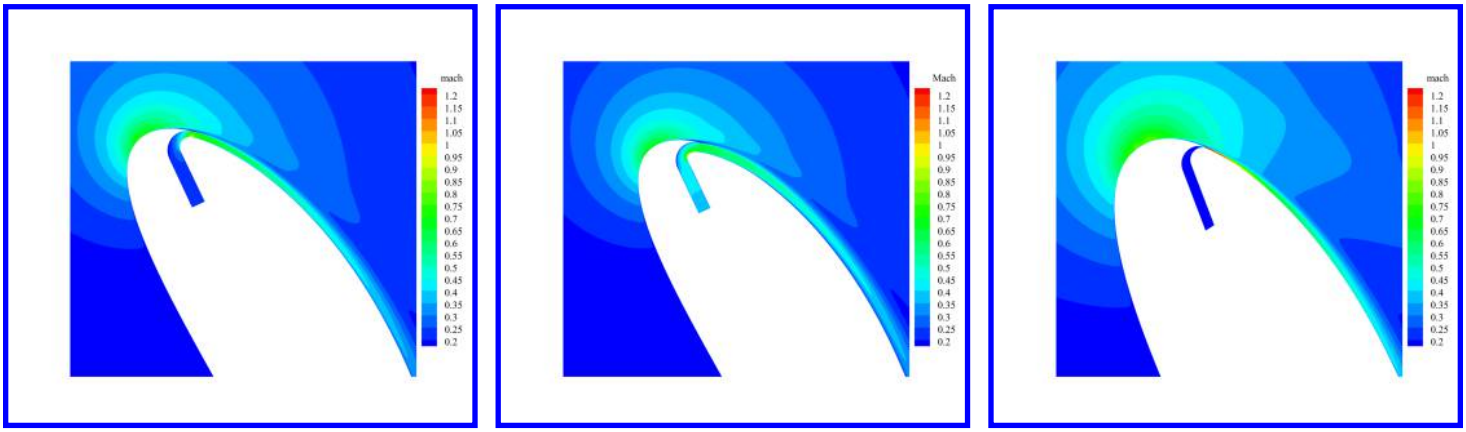

(a) CFJ 1 (b) CFJ 2 (c) CFJ 3

Figure 9: Mach number contours zoomed in the injection region for CFJ 1, CFJ 2, and CFJ 3 airfoils at same lift coefficient.

Fig. 10 shows the lift, drag, and moment coefficients versus AoA for CFJ 2 airfoil at different C_μ. As we can see, the lift increases with the increase of C_μ. The drag is decreased with C_μ and the drag are all negative (thrust) until the airfoil is stalled. The nose down moment coefficient is increased due to the overall lift coefficient increase.

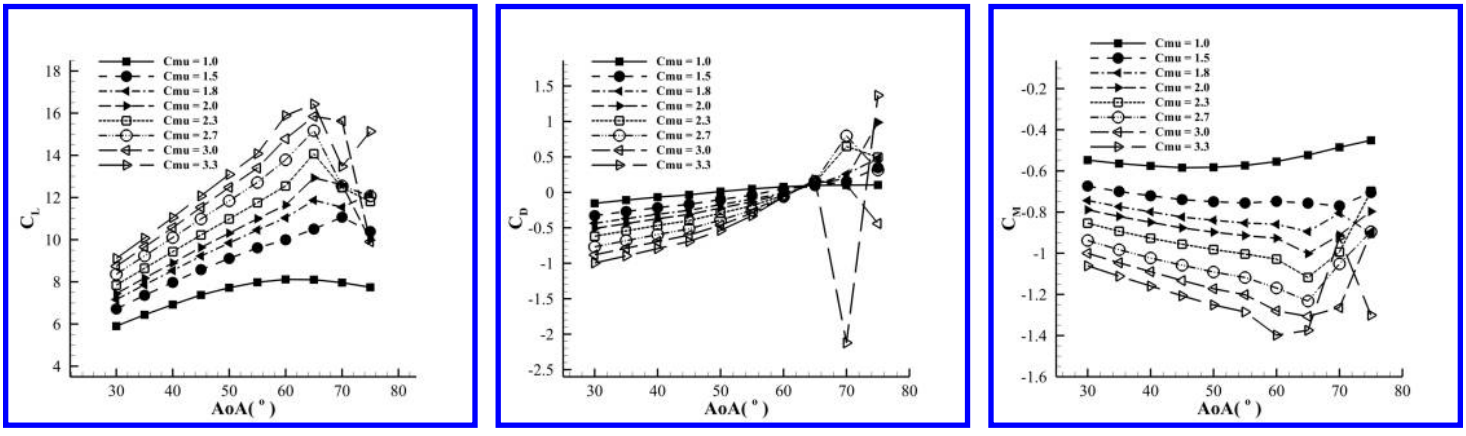

(a) (b) (c)

Figure 10: Lift, drag and moment coefficients for CFJ 2 airfoil at different C_μ.

Fig. 11 shows the Mach contours with streamlines at AoA of 65° for CFJ 2 airfoil with an increasing C_μ. Fig. 11 shows that the first stagnation point is near trailing edge on the pressure surface side. When the C_μ is greater

than 3.0 as shown in Fig. 11 (e) and (f), the second stagnation point is detached from the solid body of the airfoil and is located at the end of a vortex at the trailing edge. This is because of the ultra-high circulation similar to the potential flow of a rotating cylinder. The trailing edge vortex is like an extension of the airfoil solid body. The same phenomenon was observed first by Yang and Zha [2] for the thin injection slot CFJ airfoil based on 2D RANS simulation. Fig. 11 indicates that the same phenomenon exists for the CFJ airfoil with a 13 times larger injection slot size.

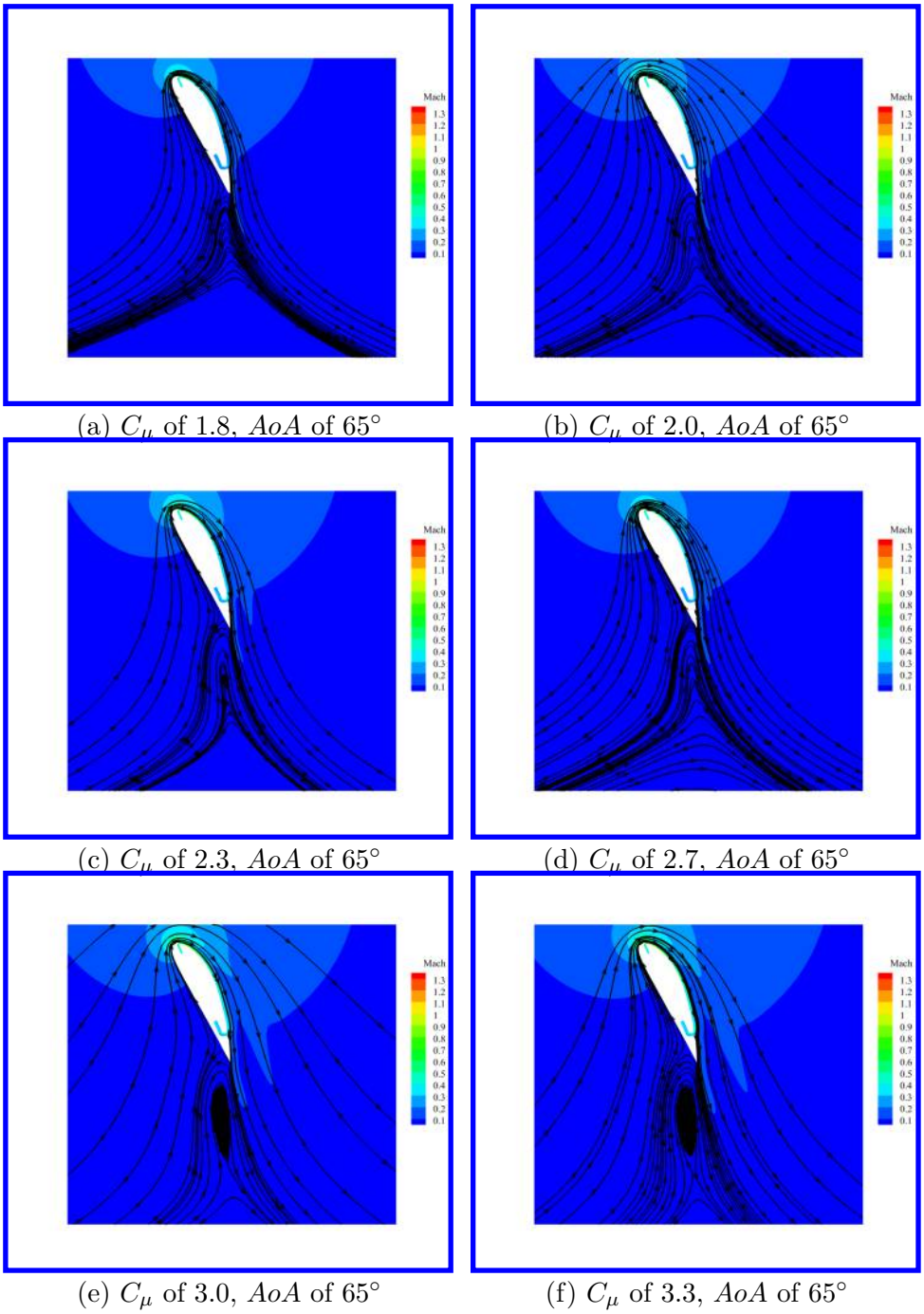

(a) C_μ of 1.8, AoA of 65° (b) C_μ of 2.0, AoA of 65°

(c) C_μ of 2.3, AoA of 65° (d) C_μ of 2.7, AoA of 65°

(e) C_μ of 3.0, AoA of 65° (f) C_μ of 3.3, AoA of 65°

Figure 11: Mach contours of stagnation points for CFJ airfoil 2 at same AoA of 65° and at different C_μ.

Yang and Zha [2] observed that there are 4 counter-rotating vortex layers when the SLC occurs for the CFJ 3 airfoil. We want to know if the same vortex structures also exist for a CFJ airfoil with large injection slot as the CFJ 2. As the reference, the vortex structures of the baseline NACA 6421 airfoil with no flow control is presented in Fig. 12 from low AoA to high AoA when the airfoil is stalled. Since NACA 6421 is fairly thick airfoil, the flow separation starts at AoA of 6° as shown in Fig. 12 (c). Overall, the vortex structure is fairly simple as governed by the 2D RANS. There is only one vortex layer on the surface of the airfoil created by the boundary layer. On the suction (upper) surface, the vortex layer is clockwise. On the pressure (lower) surface, the vortex layer is counter-clockwise. The vortex layers remain the similar structure whether the flow is attached or separated.

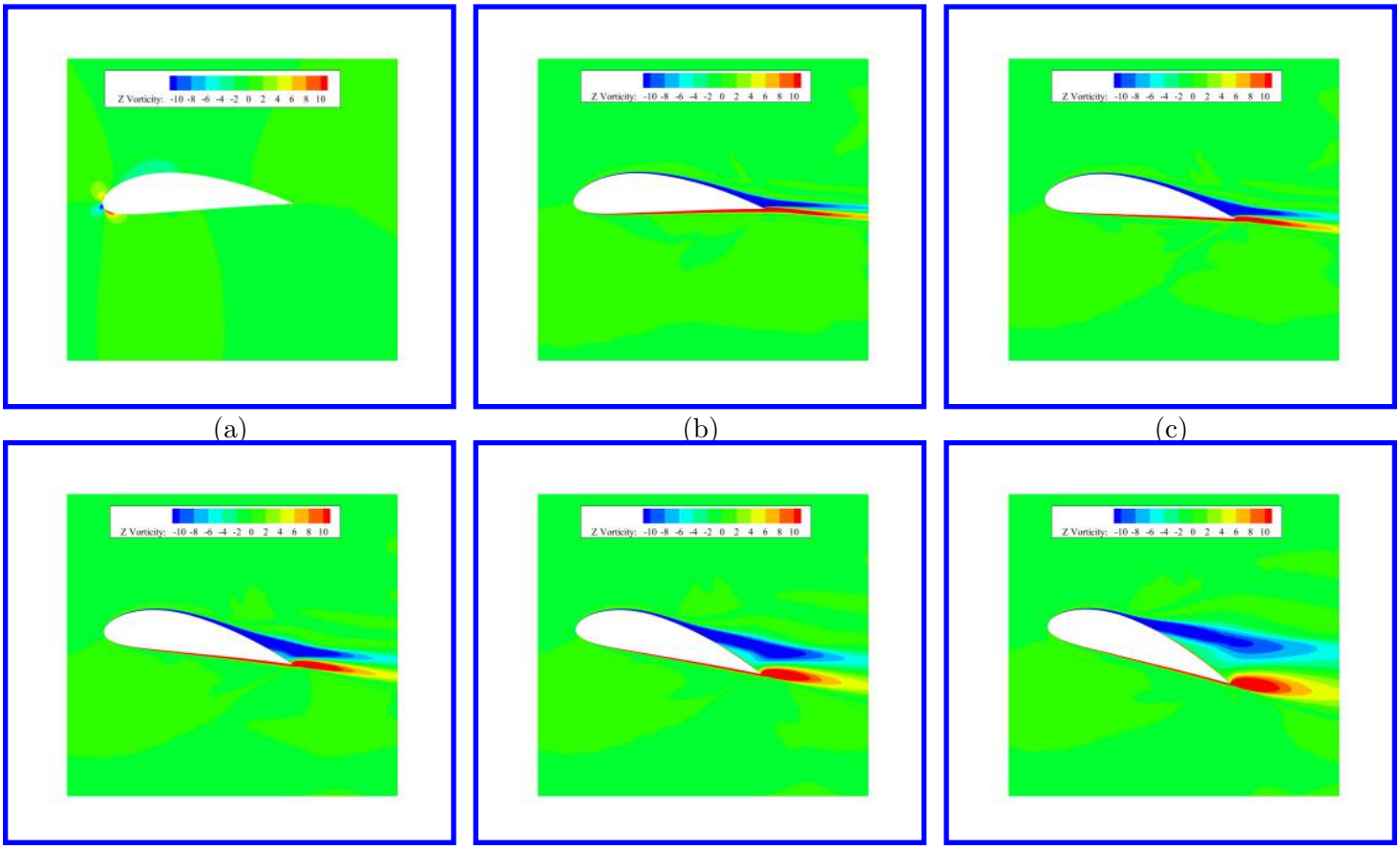

Figure 12: The vorticity for baseline airfoil at AoA of 0°, 2°, 6°, 10°, 14°, and 18°.

The vorticity contours of the CFJ 2 airfoil at different AoA and C_μ of 2.0 are shown in Fig. 13 with the AoA varied from 30° to 80°. The flow remains attached at AoA of 75° with a very minor separation at AoA of 80°. When the AoA is less than 60°, the vortex layer structures on the suction surface in the injection region remain the same. Counting from the airfoil suction wall surface to outside, there is one clockwise vortex layer (blue) on the surface of the airfoil due to the wall boundary layer, one counter-clockwise layer (red) due to the CFJ injection outside of the boundary layer, and a very thin clockwise vortex layer sledded from the leading airfoil wall surface. The last clockwise vortex layer is weak and is dissipated quickly in a short distance downstream of the injection slot. When the C_L reaches its peak at AoA of 65°, the vortex structures are dramatically changed as seen by comparing Fig. 13 (g) and (h). There are 4 layers of counter-rotating vortex as observed by Yang and Zha [2]. The second clockwise vortex layer (blue) is suddenly enlarged and trailed all the way beyond the trailing edge. The

same vortex structures remain beyond AoA of 65°. Based on the KuttaJoukowski theorem and Stokes' theorem converting a line integral to a surface integral, it can be seen that the largely increased second clockwise vortex layer contributes significantly to the ultra-high lift coefficient. More fundamental studies of the formation of the vortex is necessary.

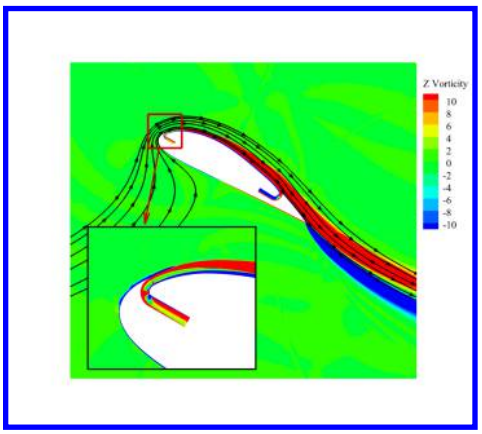

(a) C_μ of 2.0, AoA of 30°

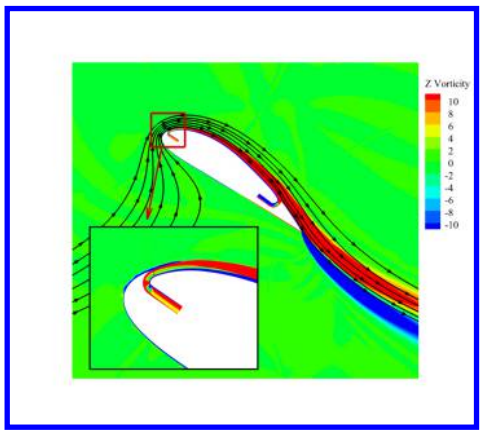

(b) C_μ of 2.0, AoA of 35°

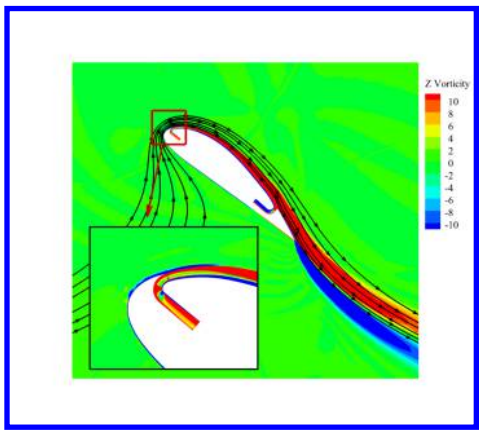

(c) C_μ of 2.0, AoA of 40°

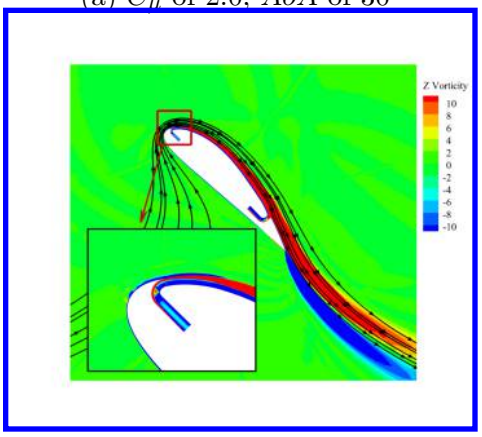

(d) C_μ of 2.0, AoA of 45°

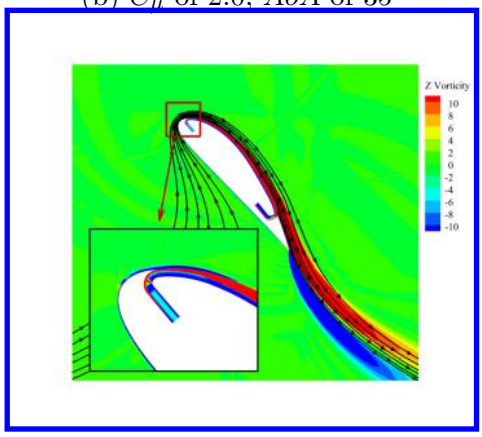

(e) C_μ of 2.0, AoA of 50°

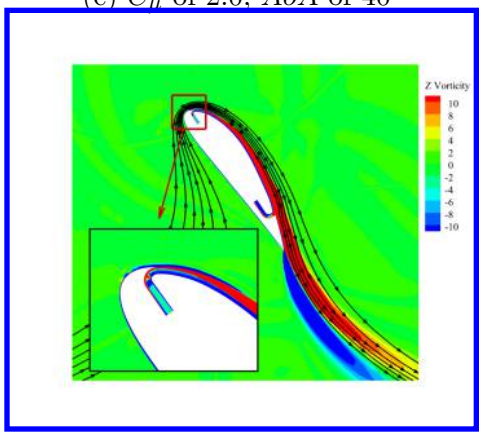

(f) C_μ of 2.0, AoA of 55°

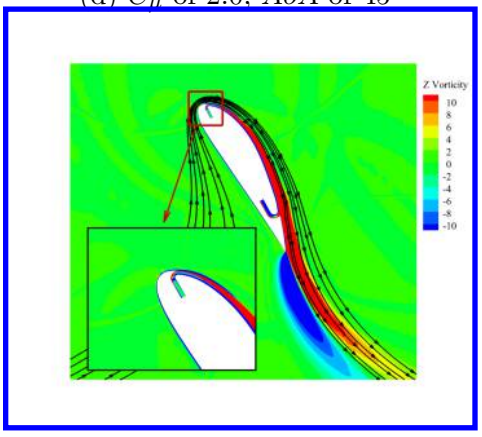

(g) C_μ of 2.0, AoA of 60°

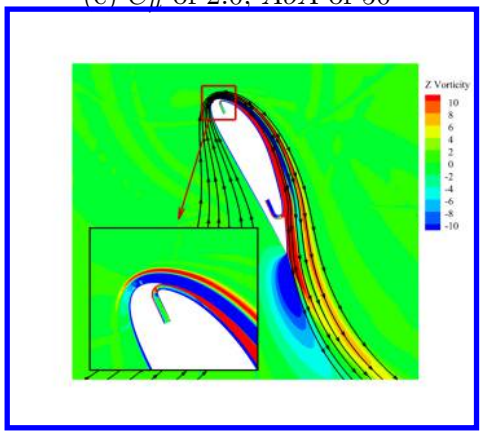

(h) C_μ of 2.0, AoA of 65°

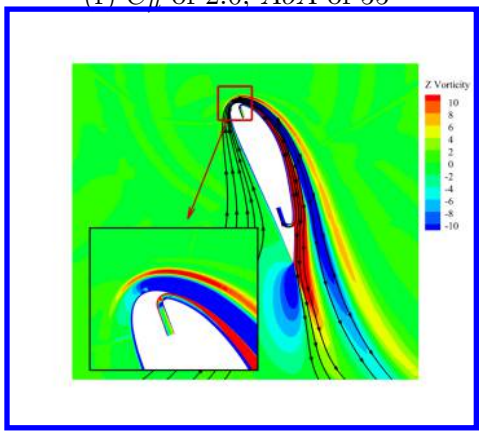

(i) C_μ of 2.0, AoA of 70°

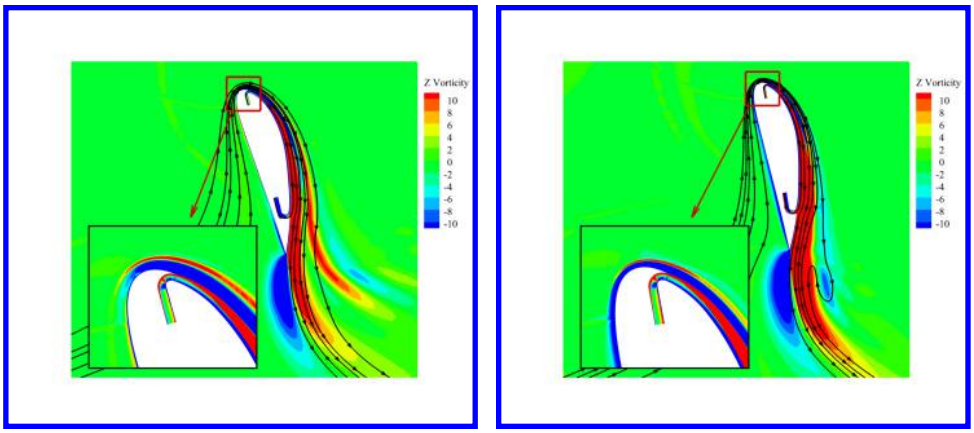

(j) C_μ of 2.0, AoA of 75° (k) C_μ of 2.0, AoA of 80°

Figure 13: The vorticity for CFJ 2 airfoil at AoA of 30° to 80° (step value of 5°) at C_μ of 2.0.

The 4 counter rotating vortex layers are reflected by the velocity vector profiles as shown in Fig. 14, which has the vorticity contours background with velocity vector profiles at 8 locations. The velocity vector profile at the station 1 and 2 clearly show the vortex rotation direction. Near the wall, the boundary layer enhanced by the injection jet generates a strong clockwise vortex layer (blue). Due to the mixing, at the edge of the boundary layer and the jet, there is a thin uniform velocity layer that has zero vorticity. The jet mixing with the flow outside of the jet decreases the velocity at the edge and forms a counter-clockwise vortex layer (red). The flow outside of the jet is induced by the jet and is accelerated by the centrifugal force, which creates a clockwise vortex layer (the wide blue layer). Beyond the 2nd clockwise vortex layer, the flow goes through a vorticity free uniform velocity layer, beyond which, the velocity is decreased and creates a counter-clockwise vortex layer (the last red layer).

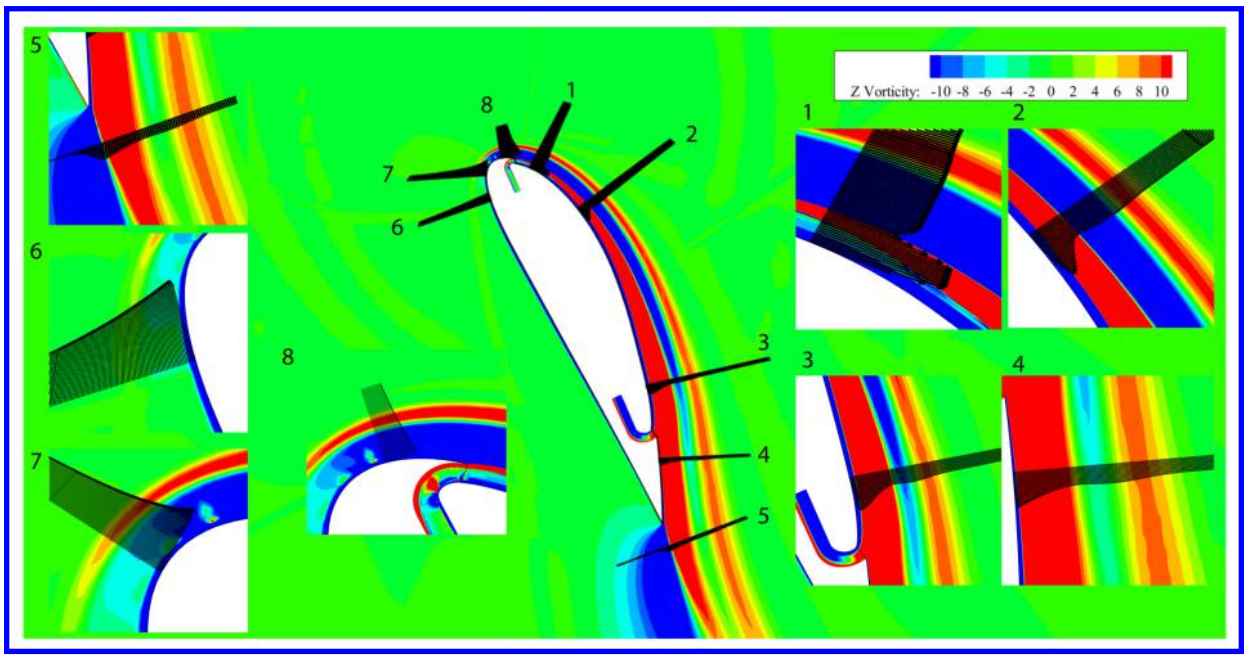

Figure 14: The vorticity profile for CFJ 2 airfoil at AoA 65.

8 Conclusion

This paper studies the super-lift coefficient of co-flow jet airfoil and its power consumption. An optimized CFJ airfoil for cruise with enlarged injection slot size by 13 times can achieve higher maximum lift coefficient than the baseline CFJ airfoil, but at substantially lower power consumption. The reason is that the CFJ power consumption is determined linearly by the mass flow rate, but exponentially by the total pressure ratio. The larger injection slot size yields greater C_μ, higher mass flow rate, and lower injection jet velocity, which generates much smaller flow energy loss, lower total pressure ratio, and hence substantially reduces the CFJ power consumption. For example, at a C_{Lmax} of 9, the total pressure ratio is reduced from 4.2 to 1.3 when the injection slot size is increased from 0.09%C to 1.17%C. The power coefficient is reduced by 5 times. Such phenomenon applies to all active flow control using fluidic actuators. The flow vortex structures are studied by comparing the flow from AoA of 30° to 80°. The flows are all attached. At an AoA below 60°, the vortex structures on the CFJ airfoil suction surface are primarily three layers, 1) a clockwise layer due to the wall boundary layer; 2) a counter-clockwise layer due to the high speed jet; and 3) the second clockwise vortex layer shed from the leading wall boundary layer, which is dissipated quickly downstream of the injection slot. However, when the flow reaches the stall AoA of 65° with the maximum lift coefficient and adverse pressure gradient, the second clockwise vortex layer is erupted with a substantially enlarged area, which contributes significantly to the ultra-high lift generation. The vortex structures become four counter-rotating vortex layers as previously observed by Yang and Zha [2]. The overall conclusion is that a CFJ airfoil with a large injection slot size is preferred. It is as effective to enhance lift, generate thrust, and increase stall AoA, but at a substantially lower power consumption. It makes the same CFJ airfoil with fixed geometry applicable to the whole flight envelop from takeoff/landing to cruise.

9 Acknowledgment

The simulations are conducted on Pegasus supercomputing system at the Center for Computational Sciences at the University of Miami.

References

[1] Lefebvre, A. and Zha, G.-C., "Trade Study of 3D Co-Flow Jet Wing for Cruise and Takeoff/Landing Performance." AIAA Paper 2016-0570, AIAA SCITECH2016, AIAA Aerospace Science Meeting, San Diego, CA, 4-8 January 2016.

[2] Yunchao Yang and Gecheng Zha, "Super-Lift Coefficient of Active Flow Control Airfoil: What is the Limit?." AIAA Paper 2017-1693, AIAA SCITECH2017, 55th AIAA Aerospace Science Meeting, Grapevine, January 9-13 2017.

[3] A. Smith, "High-Lift Aerodynamics," *Journal of Aircraft*, vol. 12, pp. 501–530, 1975.

[4] G.-C. Zha, Y.-C. Yang, Y. Ren, and B. McBreen, "Super-lift and thrusting airfoil of coflow jet-actuated by micro-compressors." AIAA Paper 2018-3061, AIAA AVIATION 2018, Atlanta, GA , 25 - 29 June 2018.

[5] G.-C. Zha, W. Gao, and C. Paxton, "Jet Effects on Co-Flow Jet Airfoil Performance," *AIAA Journal, No. 6,*, vol. 45, pp. 1222–1231, 2007.

[6] B. P. E. Dano, G.-C. Zha, and M. Castillo, "Experimental Study of Co-Flow Jet Airfoil Performance Enhancement Using Micro Discreet Jets." AIAA Paper 2011-0941, 49th AIAA Aerospace Sciences Meeting, Orlando, FL, 4-7 January 2011.

[7] Lefebvre, A. and Dano, B. and Bartow, W. and Di Franzo, M. and Zha, G.-C., "Performance Enhancement and Energy Expenditure of Co-Flow Jet Airfoil with Variation of Mach Number." AIAA Paper 2013-0490, AIAA Journal of Aircraft, DOI: 10.2514/1.C033113, 2016.

[8] P. R. Spalart and S. R. Allmaras, "A one-equation turbulence model for aerodynamic flows," in *30th Aerospace Sciences Meeting and Exhibit, Aerospace Sciences Meetings, Reno, NV, USA, AIAA Paper 92-0439*, 1992.

[9] Y.-Q. Shen and G.-C. Zha, "Large Eddy Simulation Using a New Set of Sixth Order Schemes for Compressible Viscous Terms ," *Journal of Computational Physics*, vol. 229, pp. 8296–8312, 2010.

[10] Zha, G.C., Shen, Y.Q. and Wang, B.Y., "An improved low diffusion E-CUSP upwind scheme ," *Journal of Computer and Fluids*, vol. 48, pp. 214–220, Sep. 2011.

[11] Y.-Q. Shen and G.-Z. Zha , "Generalized finite compact difference scheme for shock/complex flowfield interaction," *Journal of Computational Physics*, vol. doi:10.1016/j.jcp.2011.01.039, 2011.

[12] Shen, Y.-Q. and Zha, G.-C. and Wang, B.-Y., " Improvement of Stability and Accuracy of Implicit WENO Scheme," *AIAA Journal*, vol. 47, No. 2, pp. 331–344, 2009.

[13] Shen, Y.-Q. and Zha, G.-C. and Chen, X.-Y., " High Order Conservative Differencing for Viscous Terms and the Application to Vortex-Induced Vibration Flows," *Journal of Computational Physics*, vol. 228(2), pp. 8283–8300, 2009.

[14] Shen, Y.-Q. and Zha, G.-C. , " Improvement of the WENO Scheme Smoothness Estimator," *International Journal for Numerical Methods in Fluids*, vol. DOI:10.1002/fld.2186, 2009.

[15] G.-C. Zha and E. Bilgen, "Numerical Study of Three-Dimensional Transonic Flows Using Unfactored Upwind-Relaxation Sweeping Algorithm," *Journal of Computational Physics*, vol. 125, pp. 425–433, 1996.

[16] B.-Y. Wang and G.-C. Zha, "A General Sub-Domain Boundary Mapping Procedure For Structured Grid CFD Parallel Computation," *AIAA Journal of Aerospace Computing, Information, and Communication*, vol. 5, No.11, pp. 2084–2091, 2008.

[17] Y.-Q. Shen, G.-C. Zha, and B.-Y. Wang, "Improvement of Stability and Accuracy of Implicit WENO Scheme ," *AIAA Journal*, vol. 47, pp. 331–344, 2009.

[18] E. M. Greitzer, C. S. Tan, and M. B. Graf, *Internal Flow*. Cambridge University Press, 2004.

[19] Wang, Yang and Zha, G.-C., "Study of 3D Co-Flow Jet Wing Induced Drag and Power Consumption at Cruise Conditions." AIAA Paper 2019-0034, AIAA Scitech Forum 2019, San Diego, California, January 7-11, 2019.

[20] Wang, Yang and Zha, G.-C., "Study of Mach Number Effect for 2D Co-flow Jet Airfoil at Cruise Conditions." Proceeding AIAA Paper 2019, AIAA AVIATION Forum 2019, AIAA Aviation and Aeronautics Forum and Exposition, Dallas, Texas, June 17-21, 2019.